The Isotopic Composition of Present-Day Antarctic Snow in a Lagrangian Atmospheric Simulation*

M. M. HELSEN, R. S. W. VAN DE WAL, AND M. R. VAN DEN BROEKE

Institute for Marine and Atmospheric Research Utrecht, Utrecht, Netherlands

(Manuscript received 5 December 2005, in final form 5 June 2006)

ABSTRACT

The isotopic composition of present-day Antarctic snow is simulated for the period September 1980–August 2002 using a Rayleigh-type isotope distillation model in combination with backward trajectory calculations with 40-yr European Centre for Medium-Range Weather Forecasts (ECMWF) Re-Analysis (ERA-40) data as meteorological input. Observed spatial isotopic gradients are correctly reproduced, especially in West Antarctica and in the coastal areas. However, isotopic depletion of snow on the East Antarctic plateau is underestimated, a problem that is also observed in general circulation models equipped with isotope tracers. The spatial isotope–temperature relation varies strongly, which indicates that this widely used relation is not applicable to all sites and temporal scales. Spatial differences in the seasonal amplitude are identified, with maximum values in the Antarctic interior and hardly any seasonal isotope signature in Marie Byrd Land, West Antarctica. The modeled signature of deuterium excess remains largely preserved during the last phase of transport, though the simulated relation of deuterium excess with $\delta^{18}O$ suggests that parameterizations of kinetic isotopic fractionation can be improved.

1. Introduction

Polar ice sheets are valuable archives of paleoclimatic information (e.g., North Greenland Ice Core Project Members 2004; EPICA Community Members 2004). An often used proxy for past temperature (T) is the isotopic concentration of HDO and/or $H_2^{18}O$ in the ice [usually expressed as δD and $\delta^{18}O$ in parts per thousand (‰) with respect to the deviation from the Vienna Standard Mean Ocean Water (VSMOW)]. A significant spatial correlation between the isotopic composition of precipitation (hereafter δ) and mean annual T over Greenland (Johnsen et al. 1989) and Antarctica (Lorius and Merlivat 1977; Dahe et al. 1994) forms the empirical basis of the use of water isotopes as a T proxy.

The Antarctic ice sheet is of particular interest since it contains the longest ice core records on earth (EPICA Community Members 2004). Moreover, due to its rather stable polar climate, it is argued that, unlike for the Greenland situation, the Antarctic spatial δ–T relation can be used as a surrogate for the δ–T relationship on a glacial–interglacial time scale (i.e., the temporal relationship: Jouzel et al. 2003). However, the spatial δ–T relation in Antarctica can vary from one place to another (e.g., Lorius and Merlivat 1977; Robin 1983; Dahe et al. 1994). Furthermore, changes in the inversion strength may obscure the validity of the spatial δ–T relation as a robust paleothermometer (Van Lipzig et al. 2002a) and, especially on shorter time scales, the stability of the temporal δ–T relation in Antarctica is uncertain owing to a lack of independent T observations or proxies. Observational data from Dronning Maud Land (DML) show that individual events lack a robust δ–T relation (Helsen et al. 2005). When accumulation rate is high enough, a seasonal cycle will be preserved in isotope records. This seasonal cycle has been used as an alternative approach to study the Antarctic δ–T relation (e.g., Van Ommen and Morgan 1997; McMorrow et al. 2001; Helsen et al. 2005). This seasonal δ–T relation often attains much lower values since the temperature in the moisture source area also displays a seasonal cycle, which hereby moderates the extra fractionation in winter.

* The European Project for Ice Coring in Antarctica Publication Number 165.

Corresponding author address: Dr. M. M. Helsen, Institute for Marine and Atmospheric Research Utrecht, P.O. Box 80000, 3508 TA Utrecht, Netherlands.
E-mail: m.m.helsen@phys.uu.nl

DOI: 10.1175/JCLI4027.1

The second-order parameter deuterium excess (d-excess = $\delta D - 8\delta^{18}O$) is determined by nonequilibrium ("kinetic") fractionation effects due to differences in diffusivity of heavy and light water molecules. These effects occur during evaporation in the oceanic source area where the sea surface temperature, wind regime, and relative humidity leave an imprint in this parameter (Merlivat and Jouzel 1979). Differences in diffusivity also play a role at low temperatures when vapor is deposited on ice crystals in a supersaturated environment with respect to ice, leading to an additional kinetic fractionation effect (Jouzel and Merlivat 1984). Based on the above, d-excess records in ice cores are assumed to contain climatic information of moisture source regions (e.g., Stenni et al. 2001; Masson-Delmotte et al. 2004).

To provide the climatic interpretation of stable water isotopes with a better physical basis, the isotopic composition of atmospheric water has been simulated using simple Rayleigh-type distillation models (e.g., Dansgaard 1964; Jouzel and Merlivat 1984; Ciais and Jouzel 1994), intermediate complexity models (e.g., Fisher and Alt 1985; Hendricks et al. 2000; Kavanaugh and Cuffey 2003), and general circulation models (GCMs) equipped with isotope tracers (e.g., Joussaume et al. 1984; Hoffmann et al. 1998; Noone and Simmonds 2002). The GCM approach has the advantage of taking into account all relevant processes of fractionation. However, owing to its complexity, it is difficult to isolate different processes. Furthermore, results from GCMs in climate mode cannot directly be compared to specific snowfall events and GCMs have limited skill with respect to precipitation in polar regions.

Rayleigh-type distillation models and intermediate complexity models are simple to interpret but badly constrained by meteorological data. Due to their descriptive nature, pathways of moisture transport are strongly simplified. To improve this, Helsen et al. (2006) used back-trajectory calculations as an input for a Rayleigh-type distillation model, which enabled comparison of fractionation model results with individual snowfall events.

Here we extend the approach of Helsen et al. (2006) to snowfall events over a 22-yr period over the entire Antarctic continent. This approach is summarized in Fig. 1 and section 2. We first calculated backward trajectories for all snowfall events over the Antarctic continent using the 40-yr European Centre for Medium-Range Weather Forecasts (ECMWF) Re-Analysis (ERA-40) dataset as the meteorological input for the trajectory model. For this reason, we describe some relevant features of ERA-40 in the Antarctic region (section 3a). Then, we simulated isotopic distillation along these trajectories using a modified version of the Mixed Cloud Isotopic Model (MCIM: Ciais and Jouzel 1994; Helsen et al. 2006). Results of this 22-yr model run are described and discussed for $\delta^{18}O$ (section 3b) and the spatial relation with T is described (section 3c). Model results regarding d-excess are addressed in section 3d and the modeled seasonal cycle is discussed in section 3e, followed by a general discussion and conclusions.

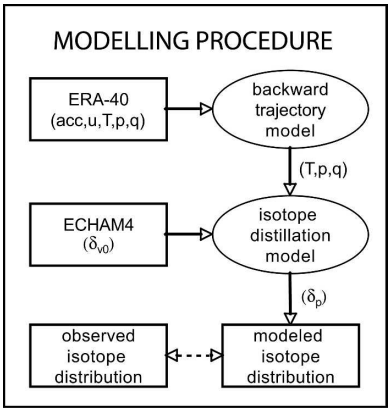

FIG. 1. Schematic outline of the modeling procedure. Backward trajectories are calculated using ERA-40 data (u: wind speed, T: temperature, p: pressure, and q: specific humidity) for all snowfall events (acc) occurring in the period 1980–2002. Isotope distillation is simulated along these trajectories using a Rayleigh-type isotope distillation model that obtains the initial isotope composition of atmospheric vapor (δ_{v0}) from a climate run of ECHAM4. Finally, the modeled isotopic distribution (δ_p) can be compared with observations.

2. Model

a. Trajectory starting points

The ERA-40 dataset constitutes the basic meteorological input for this work. The spectral resolution is T159 (corresponding to ~125-km horizontal spatial resolution) with 60 vertical levels. Here we used gridded data from this archive with a constant 1° resolution in the horizontal plane. This is the required input for the trajectory model (described below).

Based on the resolution of the input data, a network of grid points over Antarctica has been defined (Fig. 2). In the meridional direction the resolution is 1°; in the zonal direction the resolution is chosen in such a way that the grid is approximately equidistant (~111 km). More grid points are added when the coastline is crossed to ensure a fully covered continent.

Obviously, deviations from the real orography will result in errors in the simulated climate. On the Antarctic Peninsula, for instance, model resolution is insufficient to resolve the steep orography (e.g., Van Lipzig et al. 2004), and model results should be interpreted

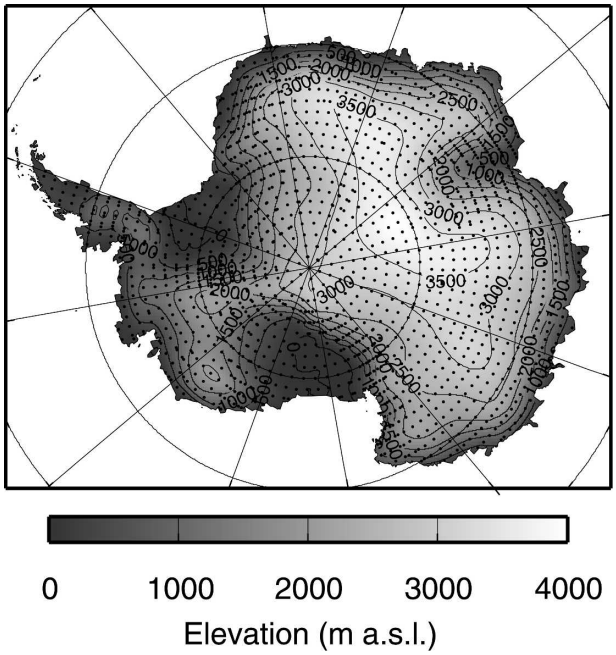

FIG. 2. Elevation of the Antarctic continent from ERA-40 (grayscale and contours) and the grid used for this simulation (dots).

with care. The grayscale in Fig. 2 indicates Antarctic orography in ERA-40. Thus, additional points are added when the elevation increases by more than 200 m over 1° in zonal direction (e.g., in the Lambert Glacier–Amery Ice Shelf region).

b. Isotopic modeling along trajectories

Daily snowfall totals (0–24-h forecast fields) are retrieved from ERA-40 for the grid described above. Although the data cover the period from 1958 to 2002, the quality changes before 1980. For example, a strong increase of Antarctic precipitation after 1980 is present in ERA-40 (Bromwich et al. 2004), probably due to the incorporation of satellite measurements into the reanalysis. For consistency, results presented here cover the 22-yr period from September 1980 to August 2002.

To simulate the isotopic composition of the accumulated snow, we use back-trajectory calculations as input for a simple Rayleigh-type isotope distillation model. Helsen et al. (2006) give an extensive description of this approach, which is only briefly addressed here.

For each day of snowfall occurring at a grid point, we calculated a 5-day backward trajectory. We used the trajectory model developed by the Royal Netherlands Meteorological Institute (Scheele et al. 1996), which computes the three-dimensional displacement of an air parcel. This model has previously been used to identify Antarctic moisture source areas (Reijmer et al. 2002).

The uncertainty in the calculated trajectories increases backward in time, resulting in a typical uncertainty of ~1000 km after five days (Stohl et al. 1995). Moreover, the advective pathway of an air parcel is not necessarily equal to the pathway of the moisture. Nevertheless, we use these trajectories because we consider them to be the best available estimate of moisture transport history for individual snowfall events.

Trajectories should ideally be calculated from arrival locations at the exact time and height of snow formation. For the timing of the snowfall events, we used 0–24-h snowfall amounts. If snowfall occurred, we chose 1200 UTC as the timing of this event and thus as the starting time for the backward trajectory calculation. To determine the vertical position of the starting point, we considered vertical profiles of cloud water content (CWC). The height of maximum CWC was used as the starting level of the back-trajectory calculation.

For the simulation of the isotope distillation process we used a modified version of the Mixed Cloud Isotopic Model (MCIM) originally described by Ciais and Jouzel 1994). This model describes the isotopic changes in a Lagrangian air parcel, quantifying the bulk effect of cloud processes on isotopic concentration. It allows vapor, liquid, and ice to coexist and interact, which is of particular importance for the simulation of *d*-excess. Three modifications of the MCIM proposed by Helsen et al. (2006) were necessary to enable the coupling of this model to the trajectory data, leading to a new model configuration (hereafter referred to as MCIM-trajs).

First, the initial isotopic composition of the moisture has to be defined. In the classical approach of a Lagrangian isotope distillation model, evaporation from the ocean surface and associated isotopic fractionation is simulated. This approach cannot be used in combination with back trajectories since the oceanic origin of the initial moisture in the air parcels is unknown. The fractionation effects of local evaporation do not yield realistic isotopic composition at the air parcel initial location (Helsen et al. 2004). To bypass this problem, we use monthly mean three-dimensional isotope fields ($\delta^{18}O$ and δD) from a 20-yr climate run of the ECMWF–Hamburg atmospheric climate model ECHAM4 (Roeckner et al. 1996; Hoffmann et al. 1998; Werner and Heimann 2002) to define the initial isotopic composition. The spectral resolution of ECHAM4 is T106 (1.1° × 1.1°) with 19 vertical levels. The use of climatological mean isotope values as the initial value for the moisture will introduce additional uncertainty in our modeling results since isotope values in single storm events show large variability compared to the

mean state (in the order of 5 ‰–10 ‰; Hoffmann et al. 1998). However, we performed sensitivity tests (not shown) by perturbing $\delta^{18}O$ values with ±5%. These tests pointed out that the influence of this error is negligible when average values over 22 years are considered.

Second, there is a discrepancy between realistic moisture transport as observed by backward trajectories and the isolated moisture transport as assumed by classical Lagrangian isotope models. In reality, air parcels often experience moisture entrainment on their way to the polar region. This entrainment is associated with isotopic recharge, that is, addition of less-depleted water vapor to the air parcel. The MCIM has been adapted at this point by assuming that any moisture increase exceeding the total available water in the air parcel is provided by ambient water vapor with an isotopic signature determined by the ECHAM4 isotope fields. Using this approach, a strong increase of specific humidity will result in near equilibration with the isotopic value of ECHAM4 at that particular location.

Third, classic Rayleigh-type isotope distillation models assume continuous saturation and rainout of moisture as a function of temperature and pressure, which can be in conflict with observed moisture transport (Helsen et al. 2004). Since condensation (and associated isotopic distillation) is not expected to occur during undersaturated conditions, we added a threshold value of relative humidity ($RH_{threshold} = 80\%$) in analogy with GCMs (Tiedtke 1993). Changes in temperature and pressure are only allowed to induce isotopic distillation if RH > 80%. The effect of this threshold is that the modeled isotopic distillation depends entirely on the difference between $T_{RH=80\%}$ and T_{final}, while in the classical approach of Rayleigh-type models, the temperature in the moisture source area was the starting point for distillation, which yielded a slightly stronger distillation.

The use of the ECHAM4 isotopic values for initial and additional moisture in our isotope model prohibits a direct interpretation of the influence of source region effects on *d*-excess. Only the effect of kinetic fractionation due to differences in diffusivity at low temperatures can be studied in MCIM-trajs. This effect is strongly dependent on the degree of supersaturation of vapor with respect to ice (S_i: Jouzel and Merlivat 1984). In our simulation this effect is parameterized as a function of T_c in a different way than in ECHAM4, leading to slightly higher values of S_i in our simulation:

$$S_{i,\mathrm{ECHAM4}} = 1.00 - 0.003T_c \quad (1)$$

$$S_{i,\mathrm{MCIMtrajs}} = 1.02 - 0.0038T_c. \quad (2)$$

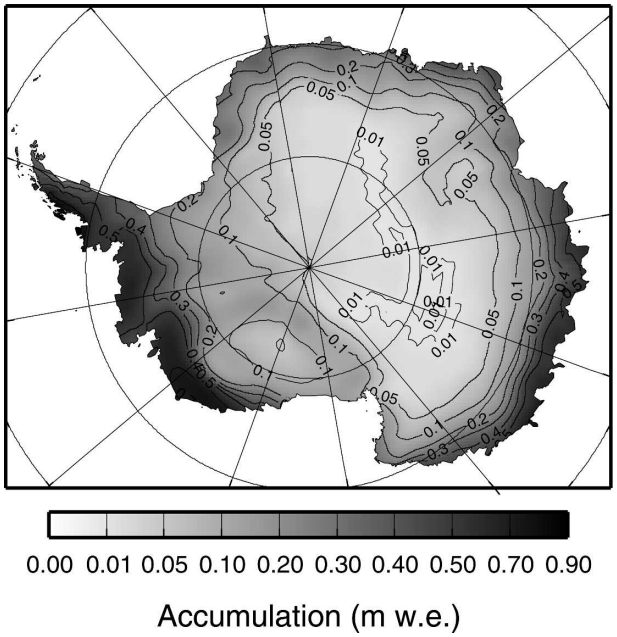

FIG. 3. Mean annual snowfall from ERA-40 for the period 1980–2002.

The simulation of *d*-excess in ECHAM4 suffers from too high values over the Antarctic Plateau (Werner et al. 2001). A possible solution of this mismatch is to increase S_i since higher values of S_i produce lower and more realistic *d*-excess values in polar precipitation (Schmidt et al. 2005). Therefore, we expect that our simulation will lead to a better description of Antarctic *d*-excess. A drawback of a higher value of S_i is that it also leads to a small reduction of isotopic distillation.

3. Results

a. Antarctic climate in ERA-40

Mean annual snowfall in Antarctica from ERA-40 is shown in Fig. 3. ERA-40 reasonably well captures the dry Antarctic interior and the wetter coastal slopes, in particular the high accumulation in the western Antarctic Peninsula and coastal Marie Byrd Land. However, ERA-40 is too dry on the East Antarctic plateau in comparison with compilations based on observations (Arthern et al. 2006) and calibrated regional climate models (Van de Berg et al. 2006). Figure 3 shows that for the driest locations in this area an annual snowfall of less than 0.01 m w.e. is simulated. Such low values of precipitation are not observed and are possibly associated with spinup problems (Genthon 2002).

Seasonality of precipitation is of major importance for the interpretation of isotope records from ice cores (e.g., Werner et al. 2000). The seasonality in ERA-40

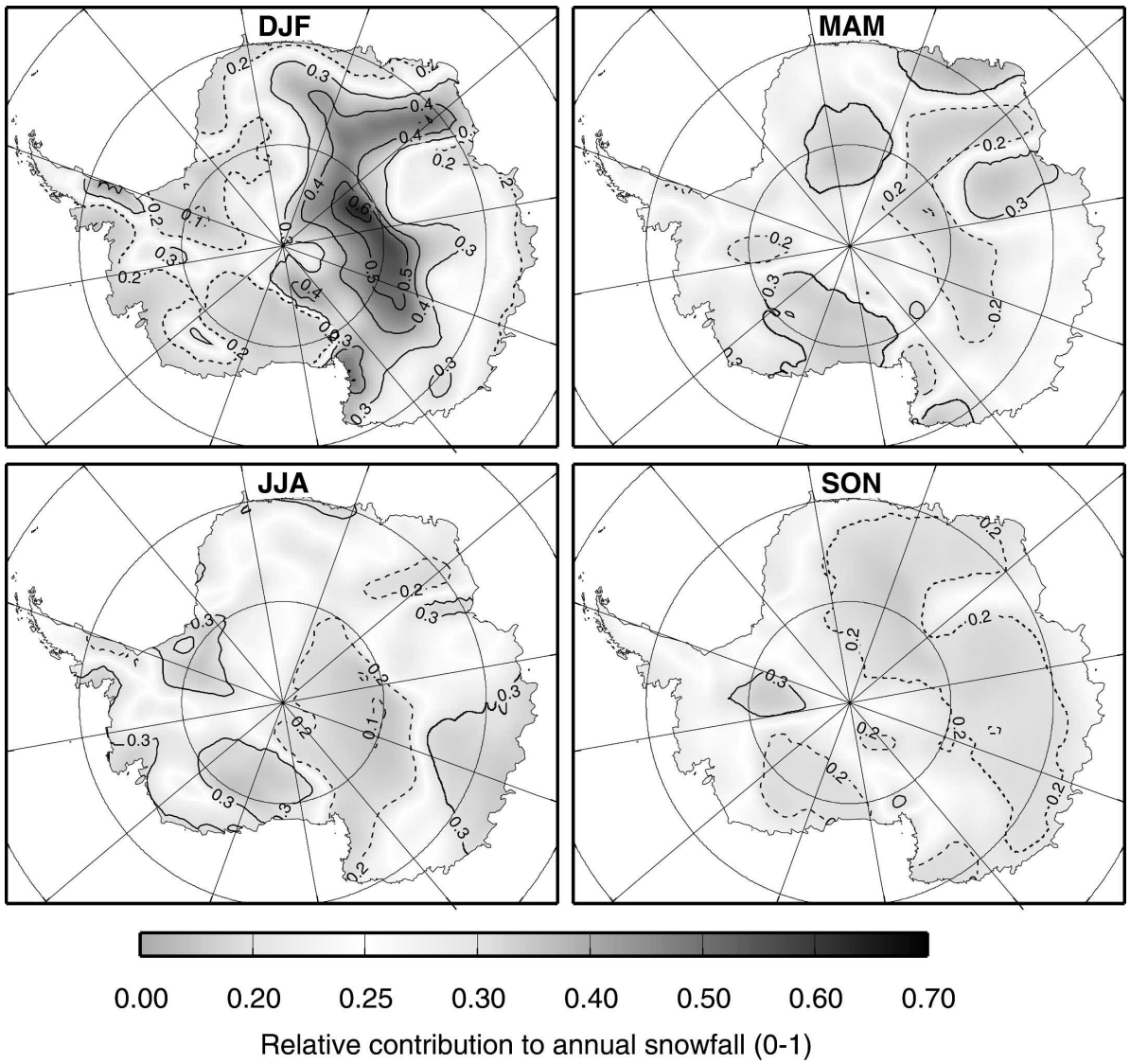

FIG. 4. Contribution of seasonal snowfall to annual mean from ERA-40 for the period 1980–2002. When a season contribution equals 0.25, no seasonal bias is introduced. A positive bias (>0.25) is indicated with solid contours; a negative bias (<0.25) has dashed contours.

snowfall is shown in Fig. 4. In the Antarctic interior, seasonal accumulation strongly peaks during the summer season [December–February (DJF)], while the coastal regions and large ice shelves receive a relatively large amount of snowfall during winter. This is not in agreement with results from regional climate models, which indicate that autumn is the dominant season for inland Antarctic precipitation (Van de Berg et al. 2006; Van Lipzig et al. 2002b). Presumably, the ECMWF model is not able to produce realistic snowfall amounts of inland precipitation during the long Antarctic winter, which causes a considerable seasonality in precipitation. This may be the reason for the underestimation of snowfall amounts over the Antarctic interior.

The mean annual surface temperature (T_s) in ERA-40 is shown in Fig. 5a. According to Genthon (2002), there is warm bias of ~5°C in ERA-40 temperature averaged over Antarctica, probably related to errors in the surface energy budget. However, he compared 2-m air temperature with 10-m firn temperature, which represents annual mean T_s. The warm bias is less when T_s is used, as is shown in Fig. 6, where modeled values of T_s from ERA-40 and ECHAM4 are compared to observed 10-m firn temperatures along three traverses: 1) the 1990 International TransAntarctic Expedition (ITAE) crossing the continent from the Antarctic Peninsula via the South Pole and Vostok to Mirny in coastal East Antarctica (Dahe et al. 1994), 2)

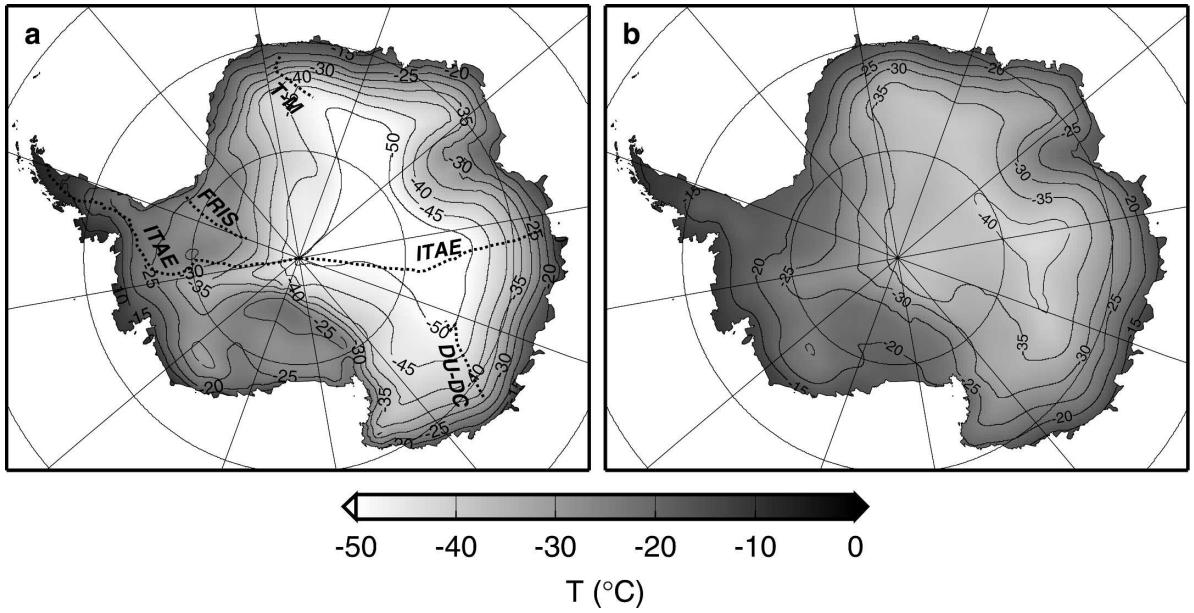

FIG. 5. (a) Mean annual T_s and (b) weighted mean values of T_c during snowfall from ERA-40 for the period 1980–2002. The dotted lines indicate traverses along which comparison with observations is shown in Figs. 6 and 9.

the 1995–96 East Antarctic traverse from Dumont d'Urville to Dome C (DU-DC; Delmotte 1997), and 3) the 1995–96 European Project for Ice Coring in Antarctica (EPICA) presite survey in DML from Troll to Site M (T-M; Van den Broeke et al. 1999; Isaksson et al. 1999). (The locations of the traverses are indicated in Fig. 5.)

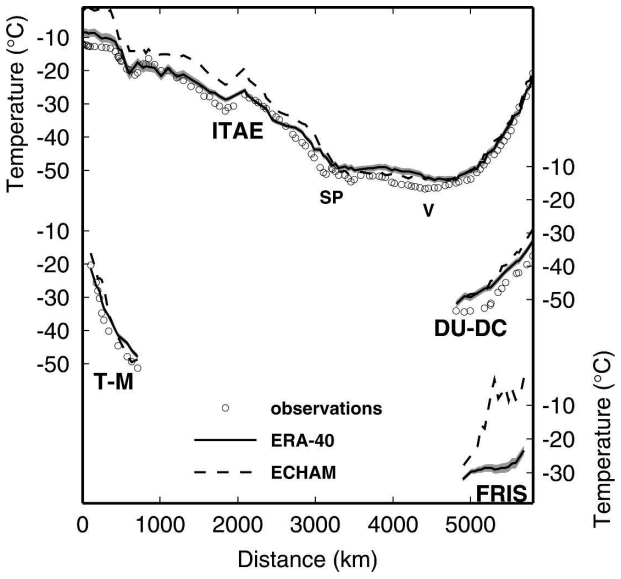

FIG. 6. Comparison of modeled (solid line: ERA-40, dashed line: ECHAM4) and observed (circles) mean annual surface temperature vs distance along the traverses indicated in Fig. 5. The standard deviation on annual mean values for ERA-40 is plotted (gray). Observed temperatures are mostly 10-m firn temperatures and are obtained from Dahe et al. (1994; ITAE), Delmotte (1997; DU-DC), and Isaksson et al. (1999; T-M); SP and V indicate the locations of the South Pole and Vostok, respectively.

In comparison with ECHAM4 (dashed line in Fig. 6), ERA-40 (solid line) performs much better in West Antarctica, but in general ERA-40 slightly overestimates T_s. Over the ice shelves, there is a major difference between ERA-40 and ECHAM4. Although no observed temperatures were available for the traverse over the Filchner Ronne Ice Shelf (FRIS), nearby measurements of 10-m firn temperature (Graf et al. 1994) indicate that ERA-40 correctly simulates the distribution of T_s and ECHAM4 overestimates T_s by >15°C. Comparable temperature deviations of ECHAM4 are detected over the Ross Ice Shelf (RIS). These large errors in T_s occur because ECHAM erroneously treats ice shelves as sea ice (Van den Broeke 1997).

To calibrate the isotope thermometer, isotopic composition of snow is often correlated to 10-m firn temperature, which is determined by long-term mean T_s. However, values of T_s in Antarctica are strongly influenced by the strength of the temperature inversion in the atmospheric boundary layer (ABL). For the isotopic composition of snow, T_s is thought to be not important. A more relevant parameter is the temperature at which water vapor is condensed to snow (T_c). The condensation process can occur at any height where water vapor pressure exceeds the saturation vapor pressure. Here we defined T_c as the temperature at the level of maximum CWC. Mean annual values of T_c, weighted

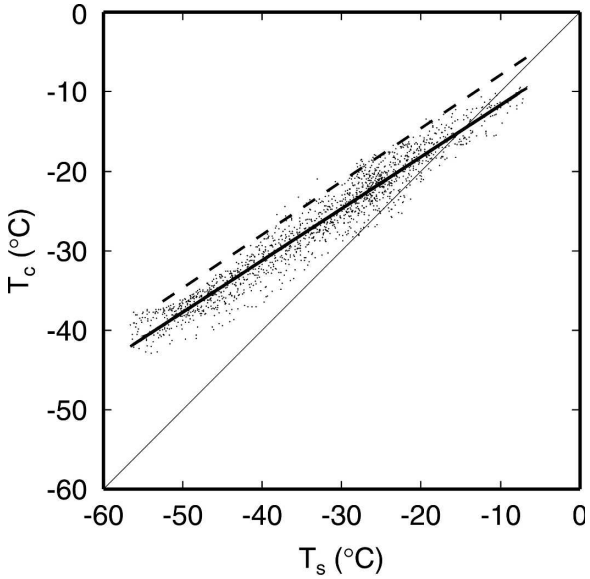

FIG. 7. Scatterplot of T_c and T_s (°C). The thick solid line is the best fit ($T_c = 0.65 - 5.2$) and the dashed line is the relation between T_s and T_i from Jouzel and Merlivat (1984).

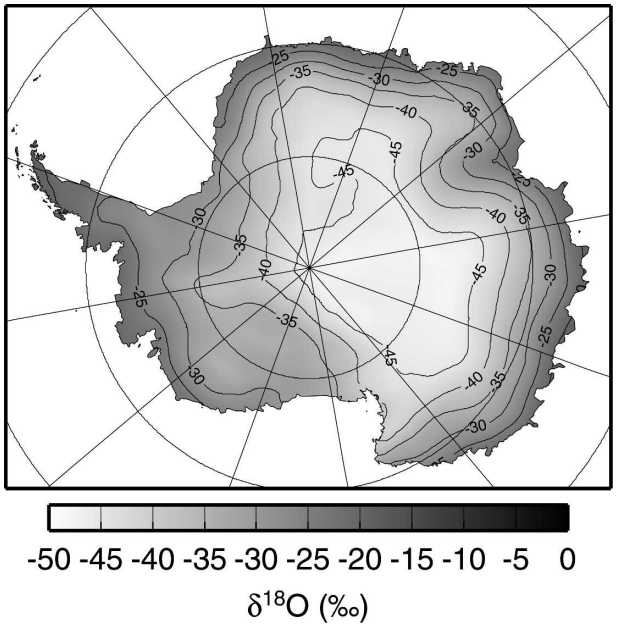

FIG. 8. Modeled mean annual $\delta^{18}O$ of snowfall for the period 1980–2002. This result is hereafter called the reference run.

with accumulation amount and occurrence, are plotted in Fig. 5b.

The scatterplot of T_s and T_c in Fig. 7 points out that T_c is generally higher than T_s except for the coastal regions. An increase of the inversion strength with decreasing T can be identified in the Antarctic interior. Jouzel and Merlivat (1984) compiled a set of observed vertical temperature profiles at several locations in Antarctica and assumed the inversion temperature (T_i) to be representative for T_c to infer a relation between T_s and T_c. This relation is plotted as the dashed line in Fig. 7. The ERA-40 data indicate that T_c is systematically lower than T_i: T_i and T_c slightly converge toward the Antarctic interior, indicating that the assumption that T_i represents T_c holds better for the Antarctic interior. In coastal regions, larger errors are introduced when using T_i as an indicator for T_c, as noted earlier by Ekaykin (2003).

To assess the quality of modeled T_c, we compared vertical temperature profiles from ERA-40 with modeled temperature profiles from a regional climate model (Reijmer et al. 2005). This comparison points out that the inversion strength in ERA-40 is somewhat weaker in comparison with the regional climate model; above the ABL, differences barely exceed 1°C.

b. Spatial distribution of $\delta^{18}O$

The mean $\delta^{18}O$ values of Antarctic precipitation as simulated with our Lagrangian isotope model are shown in Fig. 8. The main features include greatest depleted values over the Antarctic Plateau, where the lowest values of T_c occur and strongest isotopic gradients can be observed over the steep slopes of East Antarctica, along with the strongest temperature gradients.

A comparison of modeled $\delta^{18}O$ with observations along several traverses (Fig. 9) shows that modeled $\delta^{18}O$ closely resembles the observations in areas with relatively high accumulation. Over the dry Antarctic plateau, however, isotopic depletion is underestimated: $\delta^{18}O$ is correctly simulated in the Antarctic Peninsula and over the Filchner Ronne Ice Shelf. Comparing the simulated isotope distribution to compilations such as the one by Zwally et al. (1998) also shows that the depletion is underestimated by ~10 ‰ at the highest elevations. Observations of mean $\delta^{18}O$ values in Fig. 9 are generally an average value of multiple samples from the first meter of snow. This implies that these values represent different characteristic time periods depending on accumulation rate. Therefore, these values are most reliable for low-accumulation sites such as the Antarctic interior. The observations are expected to be representative values within 1 ‰ for $\delta^{18}O$, so the model significantly underestimates the depletion on the plateau.

A possible explanation for the difference is the artificial seasonality in accumulation in ERA-40, as shown in Fig. 4. However, this accounts for only a small part of the difference: if we assume an equal contribution of all seasonal accumulation, the mean modeled $\delta^{18}O$ value for Vostok precipitation would drop from −47.5 ‰ to

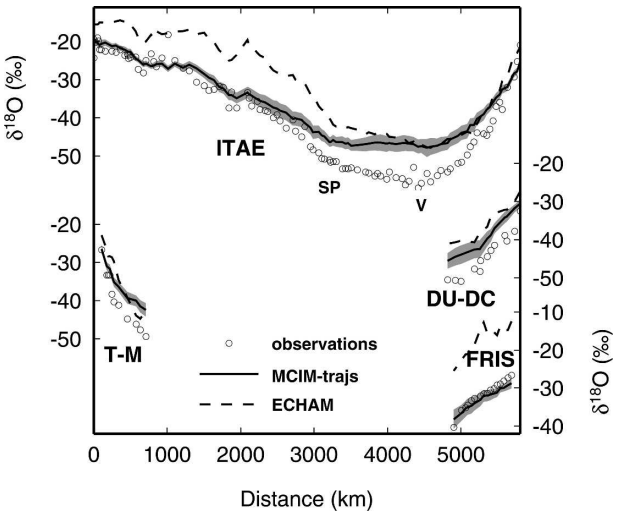

FIG. 9. As in Fig. 6, but for $\delta^{18}O$ of precipitation. Observations along the traverse crossing FRIS are obtained from Graf et al. (1999).

−48.8 ‰, which is still well above the observed −57.2 ‰. In the area with a maximum summer bias (near Dome A, Fig. 4), the modeled $\delta^{18}O$ value would decrease from −45.7 to −48.3 ‰, which is again still much higher than the observed −56 ‰ (Zwally et al. 1998). Hence, seasonality can be excluded as the main reason for the difference between observations and model results.

Another source of underestimation might originate from errors in the temperature field. However, the temperature distribution of ERA-40 does not deviate strongly from the observed temperatures (section 3a), so there is no reason to assume that the underestimation of the isotopic depletion is caused by a large temperature bias in the trajectory input data for the distillation model.

The isotopic composition of initial and additional atmospheric moisture in our simulation is determined by the ECHAM4 isotopic composition. If systematic errors in ECHAM4 exist, this will also impact our simulation. Therefore, the influence of the ECHAM4 isotope fields on our simulation is addressed in Fig. 10. The mean annual isotopic composition of Antarctic precipitation in ECHAM4 is shown in Fig. 10a. In comparison with our simulation (MCIM-trajs), ECHAM4 strongly overestimates $\delta^{18}O$ in the coastal areas, and especially over the ice shelves. The much too high temperatures over the ice shelves in ECHAM4 cause the overestimation in the ice shelf regions. In general, ECHAM4 simulates less-depleted Antarctic snow, except for a ridge ranging from DML to Dome A, where the underestimation of isotopic depletion is somewhat less than in our simulation (Fig. 10b). Other GCM simulations show a comparable underestimation of central Antarctic snow by ~10 ‰ (Noone and Simmonds 2002; Schmidt et al. 2005).

We plotted the amount of isotopic distillation that occurred exclusively along the trajectories in Fig. 10c (thereby omitting the role of ECHAM4). The absolute amount of isotopic depletion along the last 5 days of transport (the period covered by the trajectories) increases from ~10 ‰ in coastal areas to a maximum value of ~30 ‰ around Dome C. By subtracting the MCIM-trajs results (Fig. 8) from Fig. 10c, we obtain the part of the depletion caused by the use of ECHAM4 isotopic values for moisture entering the air parcels (i.e., initial plus additional moisture along transport, Fig. 10d). This latter figure shows that the simulated depletion in the area ranging from the RIS extending inland toward Dome A relies for a large part on depleted moisture from ECHAM4. The erroneous high $\delta^{18}O$ values in the ECHAM4 simulation over the RIS area (Figs. 10a,b) indicate that moisture uptake over this region can cause an overestimation of our simulated $\delta^{18}O$ values over inland East Antarctica (i.e., downflow of the RIS). However, the use of ECHAM4 values cannot be the only reason for the underestimation of the depletion over the high Antarctic Plateau since the depletion is also underestimated in inland DML, where the initial isotopic values play a much smaller role for the final simulated isotopic value.

c. *Spatial δ–T relations*

The local spatial relationship between $\delta^{18}O$ and T_s is calculated from a regression between the 22-yr mean values of $\delta^{18}O$ and T_s of all grid points within a 250-km radius (Fig. 11a). Values are only plotted when the correlation coefficient (r) is larger than 0.7. Figure 11a shows that a large spatial variability exists in the spatial δ–T_s relation. Note that the method used here differs from the usual approach that is often based on a single traverse, following a route upward onto the local ice sheet slope. The low $\Delta\delta^{18}O/\Delta T_s$ values (and low r values) in central Antarctica are caused by small changes in isotopic composition, where T_s does show a significant gradient (Figs. 5 and 8). Maximum values of $\Delta\delta^{18}O/\Delta T$ are found over inland Victoria Land and over Vostok, where isotope gradients are high and T_s gradients low. The calculated δ–T_s relation depends somewhat on the length of the search radius: applying a search radius of 500 km reduces the variability but still shows the same general pattern.

The large-scale $\Delta\delta^{18}O/\Delta T$ values can be compared with observations that have been obtained from

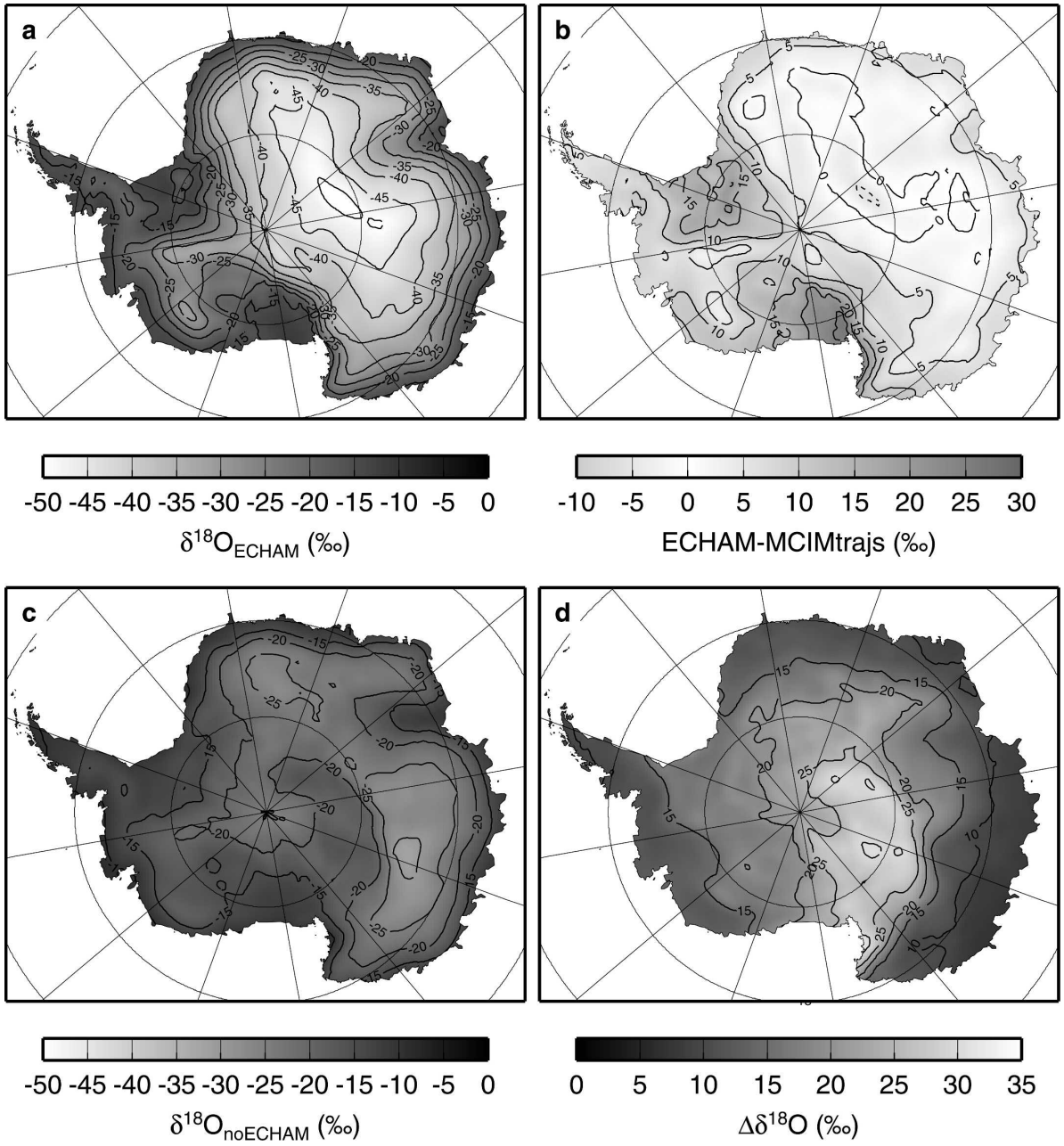

FIG. 10. (a) Modeled mean annual $\delta^{18}O$ from ECHAM4; (b) difference between (a) and reference run as shown in Fig. 8 (dashed contours indicate negative values); (c) modeled total distillation of $\delta^{18}O$ along the trajectories (no use of ECHAM for initial isotopic values); (d) difference between (c) and the reference run, showing the impact of the ECHAM4 fields on the results.

traverses (Table 1). For an objective comparison, values for the modeled spatial relationships in Table 1 are calculated using only data along the traverses, which yields somewhat higher values than obtained using a radial symmetric area. Values of simulated δ–T_s gradients are systematically lower than observed, which can again be explained by the problems in simulating the strongly depleted snow on the Antarctic Plateau.

Physically, it is more consistent to compare the spatial isotopic distribution with T_c because T_c is not affected by the inversion and T_c represents the temperature where fractionation occurs. Spatial $\Delta\delta^{18}O/\Delta T_c$ values are plotted in Fig. 11b. The pattern in Fig. 11b is comparable with the spatial relationship with T_s in Fig. 11a, but overall, $\Delta\delta^{18}O/\Delta T_c$ attains higher values. This is caused by smaller spatial gradients in T_c (Fig. 5). A

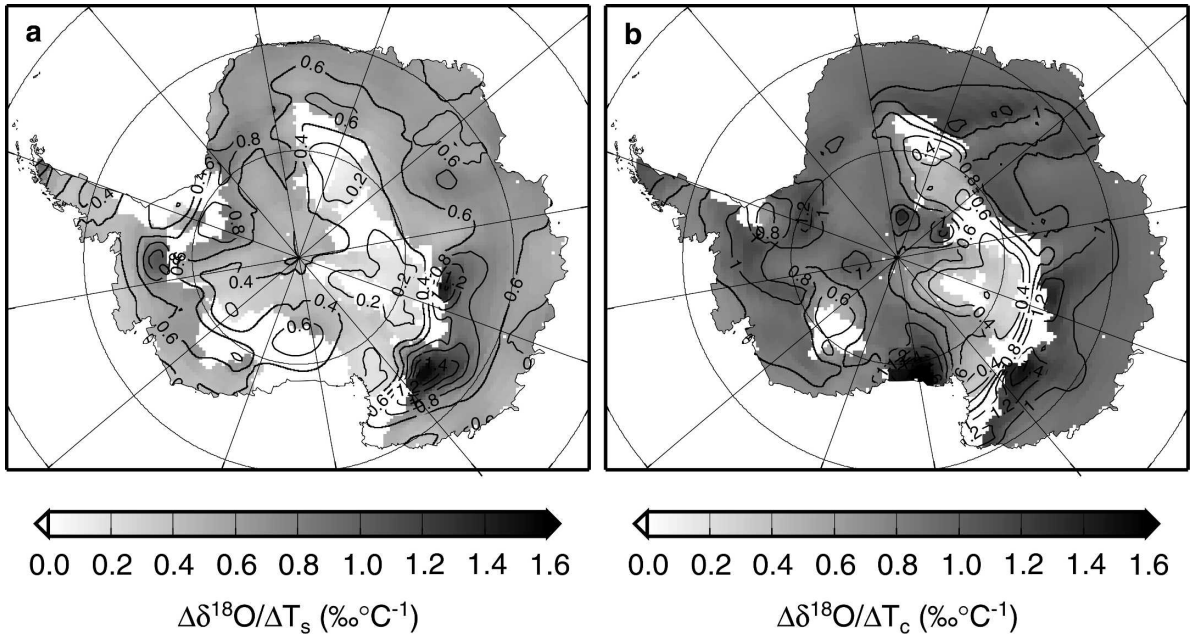

FIG. 11. Regional spatial relationships of $\delta^{18}O$ in snow with (a) T_s and with (b) T_c. Values are plotted in grayscale when $r > 0.7$.

region with low values of r is found from central–East Antarctica toward the coast in Victoria Land.

Using all grid points, modeled $\delta^{18}O$ correlates slightly better with T_c than with T_s (Table 1). A scatterplot of this relation with T_c is shown in Fig. 12a. Interestingly, the dots in this plot are grouped along three different lines (A, B, and C separated by gray dashed lines). These lines represent well-defined Antarctic regions (Fig. 12c). These different "distillation paths" are the result of differences in the isotopic composition of the vapor that enter the trajectories during transport to the deposition site. This becomes evident in Fig. 12b, showing the mean $\delta^{18}O$ values of the moisture that enters the air parcel along transport as a function of the temperature during this moisture uptake. At a comparable temperature, air parcels heading to sector C take up stronger depleted moisture compared to trajectories heading to sector A. These differences in isotopic composition of the added vapor are closely associated with the geographical location of the moisture uptake. This can be seen in Fig. 12c, where each dot represents the average location of moisture uptake for each grid point of our model domain. Evidently, moisture uptake occurs farther south for trajectories into region C compared to moisture uptake along trajectories into region B, and moisture uptake for trajectories into region A occurs even farther to the north. This is in line with Fig. 10d, which shows that this same area is strongly influenced by depleted ECHAM4 values.

Nevertheless, the mean location of the moisture up-

TABLE 1. Comparison of modeled and observed spatial isotope–temperature relationships: r values are indicated in parentheses.

	$\Delta\delta^{18}O/\Delta T_s$ (‰/°C^{-1})		$\Delta\delta^{18}O/\Delta T_c$ (‰/°C^{-1})
	Obs	$MCIM_{trajs}$	$MCIM_{trajs}$
East Antarctica		0.63 (0.90)	0.99 (0.90)
South Pole–Mirny[a]	1.03 (0.98)	0.77 (0.98)	1.25 (0.94)
T-M[b]	0.73 (0.99)	0.59 (0.99)	0.92 (0.9998)
DU-DC[c]	0.96 (0.98)	0.87 (0.99)	1.00 (0.999)
West Antarctica		0.67 (0.93)	0.98 (0.96)
Antarctic Peninsula–South Pole[a]	0.81 (0.98)	0.69 (0.99)	1.06 (0.997)
All grid points		0.61 (0.916)	0.92 (0.920)

Observations are taken from
[a] Dahe et al. (1994).
[b] Isaksson et al. (1999).
[c] Delmotte (1997).

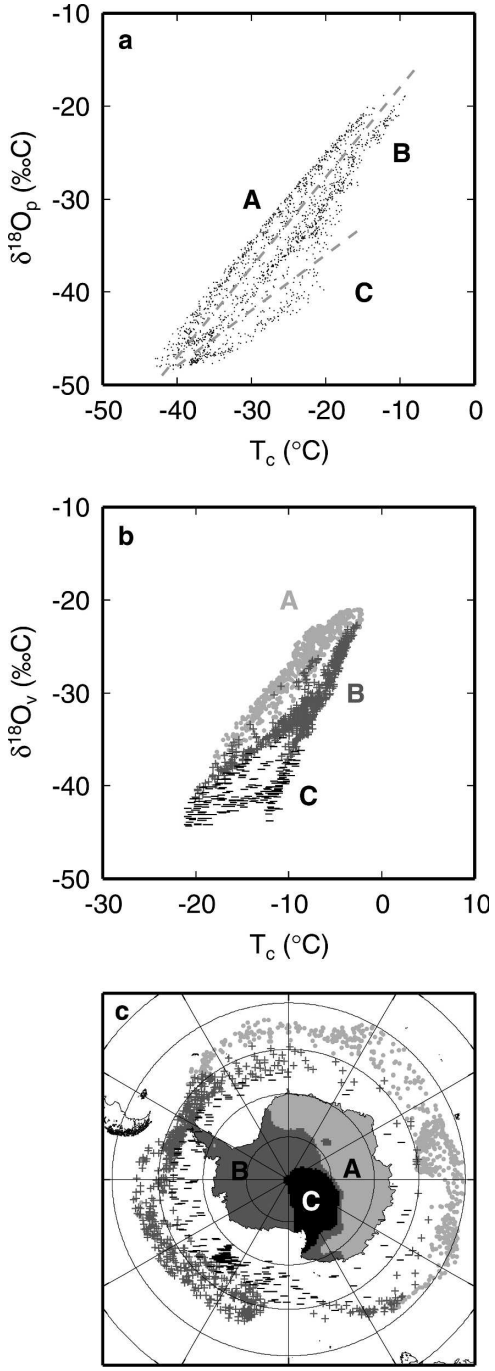

FIG. 12. (a) Scatterplot of mean $\delta^{18}O$ as a function of T_c for the entire model domain. The dashed lines divide different "distillation lines" into three sectors (A, B, and C) that represent different regions visible in (c): (b) Mean $\delta^{18}O$ values of vapor that enter the air parcel as a function of cloud temperature and reveal the same pattern as (a). The three sectors identified in (a) appear as different Antarctic regions in (c). Symbols in (c) represent the mean locations of moisture uptake for each grid point of the model domain (A: light gray dots, B: dark gray plus signs, C: black minus signs).

take cannot account for the total difference in isotopic composition as identified in Fig. 10d. The variation in the latitudinal occurrence of the moisture uptake is important as well, especially since there are large gradients in the isotopic composition over the edge of the Antarctic continent. Hence, when a large part of the moisture uptake occurs at high latitudes, the isotopic signature of moisture in air parcels will be strongly influenced by this depleted moisture. An indication of the relative contribution of this local high-latitude moisture to total moisture along the trajectories is given in Table 2, which points out that model results for region C are largely influenced by this local depleted moisture effect. This region can be characterized as a very dry area (Fig. 3), mainly as a result of a shielding effect of the geometry of the continent in combination with the steep slopes, which prevents depressions from reaching this area. Trajectories that bring snowfall to this area generally flow over West Antarctica and take up some moisture over the Ross Ice Shelf instead of over the ocean. Hence, snowfall that occurs in this area has a relatively higher contribution of local (strongly depleted) vapor to the simulated precipitation.

Since ECHAM4 isotopes are used for the isotopic composition of initial and additional moisture, associated errors can, in particular, be expected for low accumulation areas with infrequent cyclonic activity, and results for region C will be especially sensitive. This region covers an area in which the difference between simulated and observed $\delta^{18}O$ is large (Fig. 9). Lower (ECHAM4) initial $\delta^{18}O$ values would yield more realistic final results in the simulation and can be expected if ECHAM4 is colder over the ice shelves. Nonetheless, lower values of $\delta^{18}O$ in this area would also cause a larger deviation of distillation line C from lines A and B in Fig. 11c, which then confirms our conclusion that the spatial $\delta^{18}O$–T relation is not uniform over the continent.

d. Spatial pattern of d-excess

Figure 13 shows modeled *d*-excess of the snowfall. A pattern of increasing *d*-excess values toward the Antarctic interior is seen, in qualitative agreement with observed *d*-excess patterns over Antarctica (Petit et al. 1991; Dahe et al. 1994).

Figure 14a compares modeled *d*-excess with observations along the traverses of Dahe et al. (1994) and Delmotte (1997). Observed and modeled *d*-excess values correspond rather well over the Antarctic Peninsula, but modeled *d*-excess is about 5 ‰ higher than observed over the East Antarctic plateau. Thus, in spite of the (supposed) better parameterization of S_i in MCIM-trajs, *d*-excess is generally overestimated. ECHAM4

TABLE 2. Relative contribution of Antarctic (high latitude) and oceanic moisture uptake along trajectories and its mean isotopic composition. Antarctic moisture uptake is defined as increases in specific humidity (q) south of 70°S; oceanic moisture uptake is defined as increases in q north of 70°S.

	Δq (%)		$\delta^{18}O_v$ (‰)		d-excess$_v$ (‰)	
Region	Antarctic	Oceanic	Antarctic	Oceanic	Antarctic	Oceanic
A	2	98	−43.5	−23.0	27.0	9.3
B	12	88	−46.9	−24.1	31.3	9.6
C	41	59	−52.9	−26.3	37.4	10.7

performs better, especially around the South Pole, but both simulations overestimate d-excess for the DU-DC traverse. The large interannual variability of this parameter is expressed by the high standard deviation in the Antarctic interior.

In Fig. 14b, d-excess is plotted as a function of $\delta^{18}O$. Both observed and modeled d-excess show an increasing trend with decreasing $\delta^{18}O$ values. However, in both MCIM-trajs and ECHAM4, the combined d-excess–$\delta^{18}O$ relation is not modeled correctly: d-excess attains too high values with respect to the absolute value of $\delta^{18}O$ in comparison with observations. This points to more general parameterization problems of kinetic fractionation effects for the water isotopes.

The two branches of our simulation in Fig. 14b represent different relations for West (upper branch) and East (lower branch) Antarctica. As for $\delta^{18}O$, the reason for this different behavior can be found in a larger contribution of high-latitude vapor for West Antarctica, which is not only more heavily depleted in $\delta^{18}O$ but also has a much higher d-excess value (Table 2).

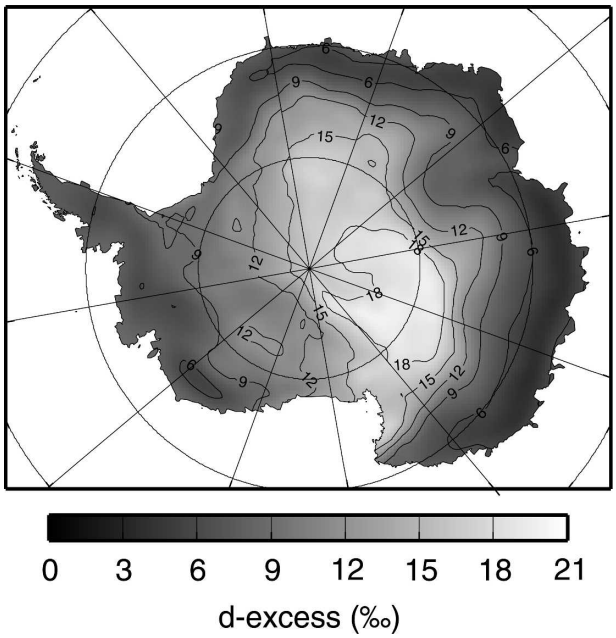

FIG. 13. Mean modeled d-excess of snowfall over the period 1980–2002.

Open circles in Fig. 14c are the observed d-excess values between Dumont d'Urville and Dome C (Delmotte 1997), and the solid circles and crosses are the d-excess values for the nearest grid points as modeled by MCIM-trajs and ECHAM4, respectively. For this particular location, MCIM-trajs produces d-excess values that are closer to the observations, but both models clearly yield too high absolute d-excess values in comparison to their $\delta^{18}O$ value.

Since the trajectories do not capture the evaporation process over the oceanic source area, this simulation cannot resolve to what extent different temperature and humidity regimes over the oceanic source are preserved in the d-excess signal. Nonetheless, it does offer the possibility to study changes in d-excess along transport paths. The gray dotted lines show d-excess as a function of $\delta^{18}O$ along the mean trajectory to each grid point. Interestingly, the modeled spatial d-excess pattern is not produced by one single air mass transporting moisture from the coast to inland Antarctica. Instead, a unique transport history (and associated d-excess evolution) exists for each location. The final difference in d-excess between each location along the traverse is present along the entire modeled transport paths in Fig. 14 and is largely determined by its initial value. Helsen et al. (2006) showed that the d-excess of this initial moisture strongly depends on the height at which vapor enters the air parcel.

These different d-excess histories along transport are an intriguing aspect of the simulation, especially for the climatic interpretation of d-excess. The dependency of d-excess on site and source conditions is often estimated using the assumption that observed spatial d-excess patterns can be used to calibrate d-excess behavior along transport (e.g., Stenni et al. 2001; Masson-Delmotte et al. 2004). Figure 14c demonstrates that this assumption does not hold in our model simulation. However, owing to the poor agreement between model results and observations, we cannot draw firm conclusions.

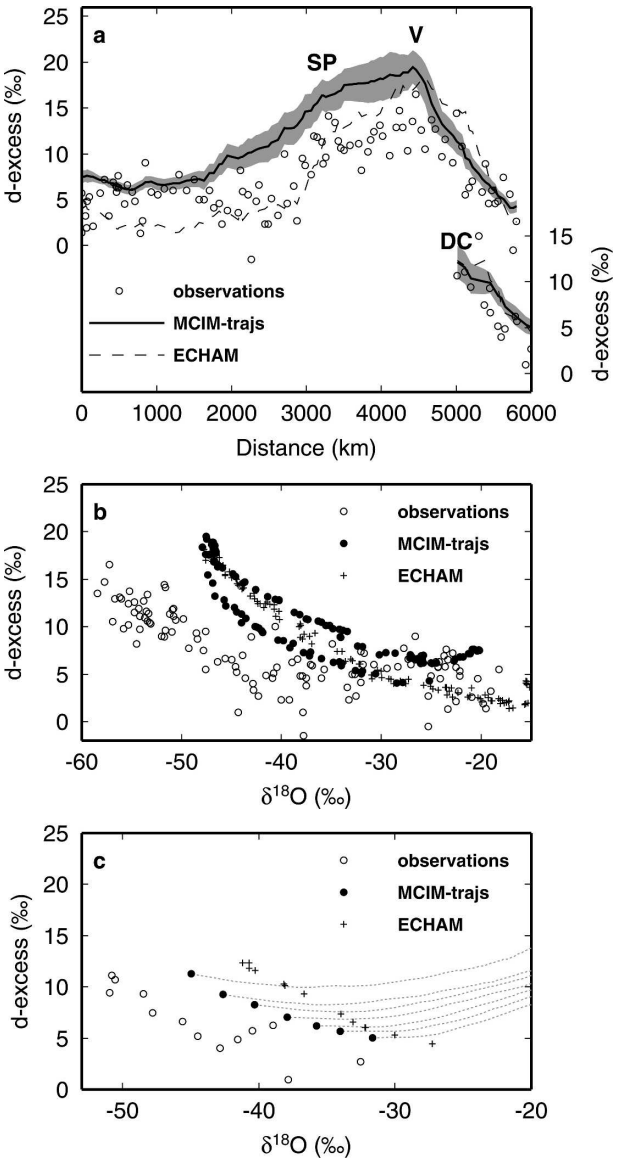

FIG. 14. Comparison of modeled and observed mean annual *d*-excess of precipitation vs (a) distance along the traverse and (b), (c) as a function of $\delta^{18}O$. For comparison, mean values from the climate run of ECHAM4 are shown as well. The standard deviation on annual mean values is plotted for our model results in (a) (gray): SP, V, and DC indicate the locations of the South Pole, Vostok, and Dome C. Observations are obtained from Dahe et al. (1994) and Delmotte (1997); see Fig. 5 for the locations of the traverses. In (c), only data from the DU-DC traverse are plotted, along with the *d*-excess values along the mean trajectories.

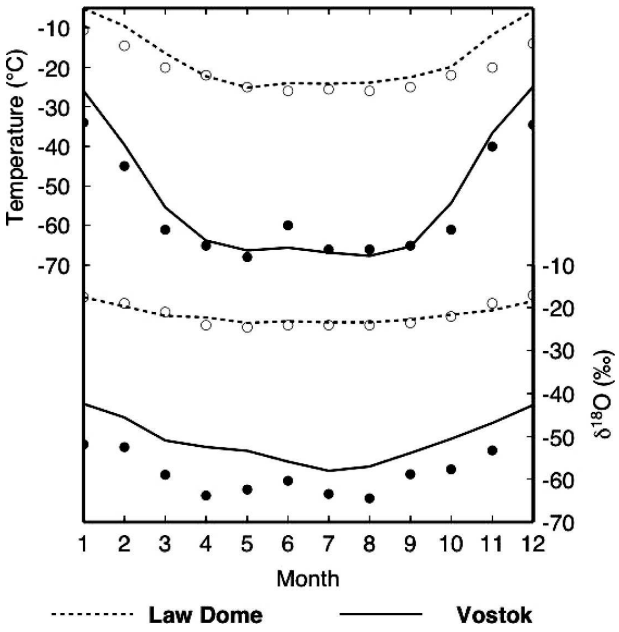

FIG. 15. Seasonal cycle of temperature and $\delta^{18}O$ for a coastal site (Law Dome, dashed line) and an inland site (Vostok, solid line). Observations (open and filled circles) are obtained from Van Ommen and Morgan (1997) and Ekaykin (2003).

The *d*-excess histories in Fig. 14c also show that a change in the parameterization of S_i would not result in a more realistic simulation since it is largely the initial imprint of *d*-excess (from ECHAM4) that determines our results instead of the kinetic fractionation effects during the final stages of transport. Moreover, increasing S_i also causes a reduction of isotopic distillation, which would result in an even larger difference between observed and modeled $\delta^{18}O$. Hence, the mutual overestimation of $\delta^{18}O$ and *d*-excess in the Antarctic interior points to parameterization problems of the water isotopes, particularly of kinetic isotope effects. This points out that the *d*-excess values over the oceanic source area in ECHAM4 are probably too high. Hence, the description of kinetic isotopic effects during evaporation over the oceanic source area can be improved.

e. The seasonal cycle

Helsen et al. (2006) showed that the seasonal cycle could be simulated reasonably well for several sites in DML. To illustrate the model performance in other Antarctic sites, we plotted the seasonal cycle of T_s and $\delta^{18}O$ at a coastal site (Law Dome) and an inland site (Vostok) in Fig. 15. The underestimation of the isotopic depletion over the Antarctic interior is again clearly visible in the Vostok results, but the seasonal amplitude is remarkably similar. Furthermore, Fig. 15 reveals no clear offset in simulated temperature.

The magnitude of the simulated seasonal cycle is shown in Fig. 16a by plotting the difference between minimum and maximum monthly mean values. A distinct pattern of increasing seasonal amplitude with increasing distance to the coast is found. Furthermore, a

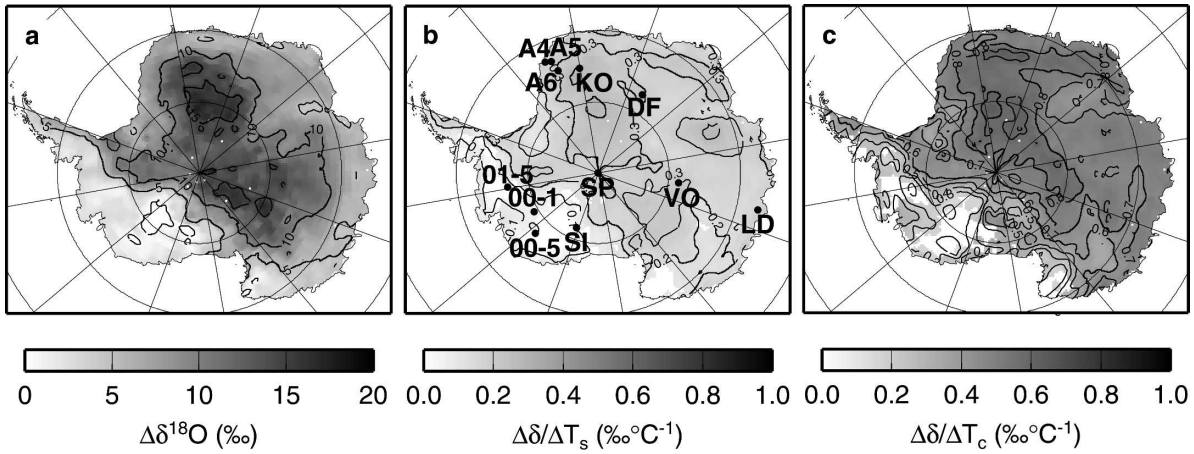

FIG. 16. (a) Seasonal difference (summer − winter) of monthly mean $\delta^{18}O$ values and associated seasonal relationships of $\delta^{18}O$ with (b) T_s and (c) T_c. Locations of sites in Table 3 are indicated with dots; A4: AWS 4, A5: AWS 5, A6: AWS 6, KO: Kohnen, DF: Dome F, LD: Law Dome, VO: Vostok, SP: South Pole, 00–1: US-ITASE 00–1, 00–5: US-ITASE 00–5, 01–5: US-ITASE 01–5, and SI: Siple Dome.

region with a surprisingly low seasonal amplitude of less than 5 ‰ is found in coastal West Antarctica.

To assess how realistic these results are, we compared the seasonal amplitudes in our model results with a number of sites from which observations are available (Table 3). In general, observations and model results both indicate smaller isotopic seasonal amplitudes in coastal areas compared to inland sites. Only in DML is the modeled increasing trend of the seasonal amplitude toward the interior not recognized in the observations. It should be mentioned that most observations are only based on a few (or even just one) years of monitoring. The West Antarctic minimum in seasonal amplitude appears to be real according to the ice core data from West Antarctica [Schneider et al. 2005; Table 3 (below)].

Figure 16b shows the relation with the seasonal tem-

TABLE 3. Comparison of seasonal isotope–temperature relationships for different Antarctic sites (locations indicated in Fig. 16); r values from regression of modeled mean monthly temperature and isotope values are indicated in parentheses. Source of observations and type of seasonal isotope measurements listed in footnote.

	$\Delta\delta^{18}O_{\text{summer–winter}}$ (‰)		$\Delta\delta^{18}O/\Delta T_s$ (‰ °C^{-1})		$\Delta\delta^{18}O/\Delta T_c$ (‰ °C^{-1})	
	Obs	$MCIM_{trajs}$	Obs	$MCIM_{trajs}$	Obs	$MCIM_{trajs}$
AWS 4[a]	14.0	7.6	0.55	0.21(0.96)	0.57	0.70(0.91)
AWS 5[a]	7.4	7.6	0.60	0.27(0.96)	0.83	0.71(0.90)
AWS 6[a]	11.8	9.7	0.67	0.30(0.95)	0.77	0.77(0.94)
Kohnen[a]	9.7	14.8	0.37	0.39(0.97)	0.49	0.86(0.98)
Dome F[b]	21.0	17.0	0.47	0.30(0.89)	1.04[h]	0.77(0.97)
Law Dome[c]	6.0	5.9	0.44	0.26(0.98)	—	0.71(0.92)
Vostok[d]	13.8	15.6	0.33	0.31(0.95)	0.97	0.81(0.97)
South Pole[e]	14.0	14.3	—	0.27(0.96)	1.40	0.71(0.91)
US-ITASE 00–1[f]	3.0	4.0	0.13	0.09(0.80)	—	0.27(0.85)
US-ITASE 01–5[f]	4.7	3.1	0.21	0.04(0.36)	—	0.26(0.61)
	$\Delta\delta D_{\text{summer–winter}}$		$\Delta\delta D/\Delta T_s$		$\Delta\delta D/\Delta T_c$	
US-ITASE 00–5[f]	15	45	0.69	0.67(0.53)	—	2.10(0.80)
Siple Dome[g]	~80	55	2.34	0.81(0.73)	—	2.60(0.65)

[a] Helsen et al. (2005): 4-yr snow pits corrected for diffusion
[b] Motoyama et al. (2005): 1 yr freshly fallen snow sampled from container roof
[c] Van Ommen and Morgan (1997): ~600-yr ice core record, corrected for diffusion
[d] Ekaykin (2003):1 yr freshly fallen snow sampled in snow traps at 1.5-m height
[e] Aldaz and Deutsch (1967): 1 yr of freshly fallen snow sampled from 0.5-m raised platform
[f] Schneider et al. (2005): ice core records
[g] Kreutz et al. (1999): 2.5-yr snow pits, not corrected for diffusion
[h] T_i is used instead of T_c

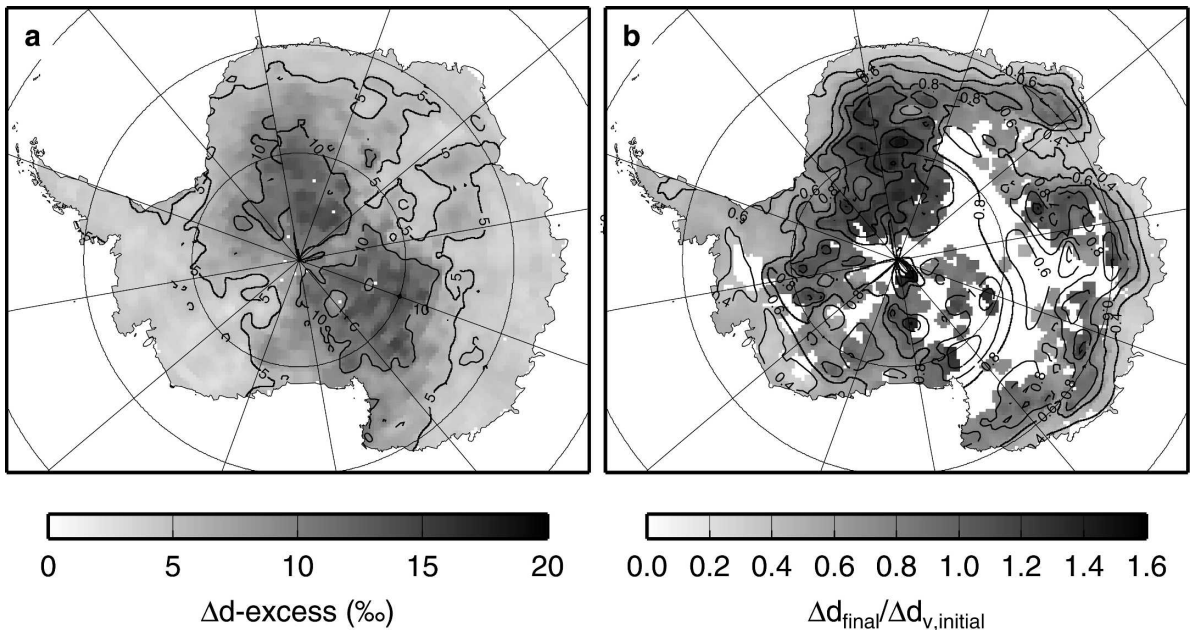

FIG. 17. (a) Seasonal *d*-excess and (b) relation of *d*-excess of the final precipitation to *d*-excess of moisture that enters the air parcel during transport. Grayscale is only plotted when $r > 0.7$.

perature cycle. Values for $\Delta\delta^{18}O/\Delta T_s$ obtained from seasonal variations are much lower than the spatial relationship (Fig. 11), in agreement with earlier studies (e.g., Van Ommen and Morgan 1997). However, the modeled values of the seasonal $\delta^{18}O$–T relation are also consequently lower than observed (Table 3). This can be related to the model's problem of producing strongly depleted $\delta^{18}O$ values, which is especially a problem for wintertime snowfall (Helsen et al. 2006); consequently, the seasonal $\delta^{18}O$–T relation is underestimated.

Figure 16c shows the seasonal relationship between $\delta^{18}O$ and T_c. Again, much higher values are obtained compared to the $\delta^{18}O$–T_s relationship. The difference is caused by the temperature inversion that develops in the Antarctic winter, which causes very low winter values for T_s but has no influence on T_c.

A poor correlation ($r < 0.7$) is obtained for large areas in West Antarctica (Marie Byrd Land), mainly because the seasonal amplitude of $\delta^{18}O$ is low for this area. Although the seasonal amplitude of T_c is also small in this area (not shown), this cannot fully explain the total difference in isotopic seasonal amplitude: also the seasonal $\delta^{18}O$–T_c gradient is much lower in Marie Byrd Land (Fig. 16c).

Since isotopic depletion of moisture is a function of the temperature difference between source and site (and not just final T_c), seasonal changes in this temperature difference may explain the observed differences. This influence is evaluated for trajectories toward the locations of both maximum and minimum seasonal amplitude. This revealed that trajectories toward Marie Byrd Land experience a similar temperature drop during both winter and summer. On the other hand, wintertime trajectories toward the Antarctic interior originate much more northward than summertime trajectories and therefore encounter a much larger temperature drop in winter, explaining the large seasonal amplitude.

The seasonal amplitude of *d*-excess is shown in Fig. 17a. Maximum values of *d*-excess occur in late autumn (May–June), and minimum values occur during early summer (November–December). Figure 14c revealed that concerning the spatial *d*-excess distribution, the *d*-excess value of the initial moisture determined to a large extent the final value. Whether this also holds for the seasonal variation is tested by calculating the regression coefficient between the initial *d*-excess value of moisture five days before arrival and the final value of the precipitation (Fig. 17b). The seasonal variability of *d*-excess in a large region ranging from Victoria Lands to Dome A remains unexplained (too low *r* values). For the remaining part of the continent, the initial moisture composition largely determines the seasonal signal in *d*-excess.

4. Discussion

The combined approach of backward trajectories and simple isotopic modeling has yielded a unique dataset

of the isotopic composition of snow in Antarctica. It is the first simulation of isotopic composition based on atmospheric reanalysis data. However, the strongly depleted values in inland Antarctica are not entirely correctly reproduced by the model. These problems are also encountered in different GCMs equipped with isotope tracers (Werner et al. 2001; Noone and Simmonds 2002; Schmidt et al. 2005), which highlights the fact that these models do not capture the Antarctic hydrological cycle (and associated isotopic fractionation processes) sufficiently well to explain all observed isotopic variability.

One of the possible causes for the discrepancy may be related to the temperature of condensation, which controls the isotopic composition of snow. In our simulation, we chose the temperature at the level of maximum condensed moisture (CWC), while in reality, condensation occurs over a large vertical range. In GCMs, the condensation process (and its vertical position) is more realistic, but this does not lead to an improved simulation of $\delta^{18}O$, so this is not a likely cause either.

The type of accumulation events can also introduce a bias in the isotopic composition. In DML, studies with automatic weather stations have revealed that accumulation is dominated by cyclonic precipitation, which only occurs a few times per year (Reijmer and Van den Broeke 2003; Helsen et al. 2005). For this type of precipitation, the definition of T_c should be appropriate. On the other hand, clear-sky precipitation is much less intermittent, and evidence exists that this type of precipitation forms a large contribution to the total precipitation on the Antarctic Plateau (Bromwich 1988; Ekaykin 2003). This type of precipitation is not accounted for in our model approach since trajectories are only calculated when condensed moisture is detected above the surface. Clear-sky precipitation likely is usually more depleted than cyclonic precipitation because it is formed at lower T and can therefore qualitatively explain the mismatch between observations and model results.

On the other hand, it is possible that monthly mean isotope fields are not representative of the average isotopic composition during storm events and thus introduce a systematic (and unknown) bias in our simulation. Especially during very intense storms, moisture that enters the air parcels can be more depleted than during "average" conditions due to earlier rainout not captured by the trajectories. This influence may be considerable in the Antarctic interior since cyclones need to be very intense in order to reach this area.

Since our simulation is based on backward trajectory calculations, simulated moisture transport was exclusively advective, and diffusive moisture transport was neglected. Only when moisture increases in trajectories occur was this process schematically described. Nevertheless, diffusive mixing along transport with (local) depleted moisture may be a key process that can account for the lack of depletion toward the Antarctic interior. However, GCMs do account for this process and do not produce results more in line with observation; so again, the matter remains unsolved.

Another mechanism not accounted for in our modeling approach, nor in GCMs, is postdepositional isotopic equilibration with atmospheric moisture (Waddington et al. 2002), which is thought to be a significant process in windy, low accumulation sites. This process cannot explain the difference of model results with freshly fallen snow samples, but may have lowered the isotopic composition in firn samples.

5. Conclusions

Modeling isotope fractionation using both simple distillation models and GCMs equipped with isotope tracers has provided valuable insight into the mechanisms behind observed global isotope variability. In this paper we presented a dataset of isotopic composition of Antarctic snow, generated using atmospheric reanalysis data combined with a trajectory model and a simple isotope model. It is demonstrated that this approach is able to reproduce most of the observed spatial gradients, and also qualitatively describes the seasonal cycle. However, isotopic depletion is underestimated for the high Antarctic Plateau.

The modeled present-day spatial $\delta^{18}O$–T relation in Antarctica appears to vary regionally, which is an indication that this widely used relation is not applicable to all sites and time scales.

Our results indicate large spatial variability in the amplitude of the seasonal isotope cycle, mostly in agreement with the observed variability. The underlying mechanisms behind these patterns can be attributed to 1) spatial variations in the seasonal amplitude of condensation temperature and 2) strong seasonal fluctuations in the latitudinal extent of the mean transport path.

Modeled d-excess qualitatively follows the observed spatial pattern but is generally higher than observations in the Antarctic interior. Analysis of the evolution of d-excess along the trajectories indicates that spatial variations in modeled d-excess are not highly influenced by the last phase of transport but are largely determined by their initial values, which are obtained from the ECHAM4 GCM. The mutual behavior of $\delta^{18}O$ and d-excess suggests that parameterization of kinetic fractionation effects can be improved.

Future work will try to identify to what extent large-scale atmospheric patterns are preserved in the isotopic composition of present-day Antarctic accumulation.

Acknowledgments. We thank Rinus Scheele for his helpful advice considering the trajectory calculations and Valérie Masson-Delmotte for her useful comments concerning the isotope modeling. Martin Werner has generously provided the ECHAM4 data and has significantly contributed to the quality of this work with fruitful discussions, just as Georg Hoffmann did. This work is a contribution to the European Project for Ice Coring in Antarctica (EPICA), a joint European Science Foundation–European Commission scientific programme, funded by the EU and by national contributions from Belgium, Denmark, France, Germany, Italy, Netherlands, Norway, Sweden, Switzerland, and the United Kingdom. The main logistic support was provided by IPEV and PNRA (at Dome C) and AWI (at Dronning Maud Land). Financial support was obtained from the Netherlands Organisation for Scientific Research (NWO) by a grant of the Netherlands Antarctic Programme.

REFERENCES

Aldaz, L., and S. Deutsch, 1967: On a relationship between air temperature and oxygen isotope ratio of snow and firn in the South Pole region. *Earth Planet. Sci. Lett.,* **3,** 267–274.

Arthern, R. J., D. P. Winebrenner, and D. G. Vaughan, 2006: Antarctic snow accumulation mapped using polarization of 4.3-cm wavelength microwave emission. *J. Geophys. Res.,* **111,** D06107, doi:10.1029/2004JD005667.

Bromwich, D. H., 1988: Snowfall in high southern latitudes. *Rev. Geophys.,* **26,** 149–168.

——, Z. Guo, L. Bai, and Q. S. Chen, 2004: Modeled Antarctic precipitation. Part I: Spatial and temporal variability. *J. Climate,* **17,** 427–447.

Ciais, P., and J. Jouzel, 1994: Deuterium and oxygen 18 in precipitation: Isotopic model, including mixed cloud processes. *J. Geophys. Res.,* **99** (D8), 16 793–16 803.

Dahe, Q., J. R. Petit, J. Jouzel, and M. Stievenard, 1994: Distribution of stable isotopes in surface snow along the route of the 1990 International Trans-Antarctic Expedition. *J. Glaciol.,* **40,** 107–118.

Dansgaard, W., 1964: Stable isotopes in precipitation. *Tellus,* **16,** 436–468.

Delmotte, M., 1997: Enregistrements climatiques à Law Dome: Variabilité pour les périodes récentes et pour la déglaciation. Ph.D. thesis, University Joseph Fourier, Grenoble, France, 298 pp.

Ekaykin, A. A., 2003: Meteorological regime of central Antarctica and its role in the formation of isotope composition of snow thickness. Ph.D. thesis, University Joseph Fourier, Grenoble, France, 122 pp.

EPICA Community Members, 2004: Eight glacial cycles from an Antarctic ice core. *Nature,* **429,** 623–628.

Fisher, D. A., and B. T. Alt, 1985: A global oxygen isotope model—Semi-empirical, zonally averaged. *Ann. Glaciol.,* **7,** 117–124.

Genthon, C., 2002: Climate and surface mass balance of the polar ice sheets in era40/era15. ECMWF Reanalysis Project Rep. Series 3, 299–316.

Graf, W., H. Moser, O. Reinwarth, J. Kipfstuhl, H. Oerter, A. Minikin, and D. Wagenbach, 1994: Snow-accumulation rates and isotopic content (^{2}H, ^{3}H) of near-surface firn from the Filchner-Ronne Ice Shelf, Antarctica. *Ann. Glaciol.,* **20,** 121–128.

——, O. Reinwarth, H. Oerter, C. Mayer, and A. Lambrecht, 1999: Surface accumulation on Foundation Ice Stream, Antarctica. *Ann. Glaciol.,* **29,** 23–28.

Helsen, M. M., R. S. W. Van de Wal, M. R. Van den Broeke, E. R. T. Kerstel, V. Masson-Delmotte, H. A. J. Meijer, C. H. Reijmer, and M. P. Scheele, 2004: Modelling the isotopic composition of snow using backward trajectories: A particular accumulation event in Dronning Maud Land, Antarctica. *Ann. Glaciol.,* **39,** 293–299.

——, ——, ——, D. Van As, H. A. J. Meijer, and C. H. Reijmer, 2005: Oxygen isotope variability in snow from western Dronning Maud Land, Antarctica and its relation to temperature. *Tellus,* **57B,** 423–435.

——, ——, ——, V. Masson-Delmotte, H. A. J. Meijer, M. P. Scheele, and M. Werner, 2006: Modeling the isotopic composition of Antarctic snow using backward trajectories: Simulation of snow pit records. *J. Geophys. Res.,* **111,** D15109, doi:10.1029/2005JD006524.

Hendricks, M. B., D. J. DePaolo, and R. C. Cohen, 2000: Space and time variation of δ^{18}O and δD in precipitation: Can paleotemperature be estimated from ice cores? *Global Biogeochem. Cycles,* **14,** 851–861.

Hoffmann, G., M. Werner, and M. Heimann, 1998: Water isotope module of the ECHAM atmospheric general circulation model: A study on time scales from days to several years. *J. Geophys. Res.,* **103** (D14), 16 871–16 896.

Isaksson, E., M. R. Van den Broeke, J.-G. Winther, L. Karlöf, J. F. Pinglot, and N. Gundestrup, 1999: Accumulation and proxy temperature variability in Dronning Maud Land, Antarctica, determined from shallow firn cores. *Ann. Glaciol.,* **29,** 17–22.

Johnsen, S. J., W. Dansgaard, and J. W. C. White, 1989: The origin of Arctic precipitation under present and glacial conditions. *Tellus,* **41B,** 452–468.

Joussaume, J., R. Sadourny, and J. Jouzel, 1984: A general circulation model of water isotope cycles in the atmosphere. *Nature,* **311,** 24–29.

Jouzel, J., and L. Merlivat, 1984: Deuterium and oxygen 18 in precipitation: Modeling of the isotopic effects during snow formation. *J. Geophys. Res.,* **89** (D7), 11 749–11 757.

——, F. Vimeux, N. Caillon, G. Delaygue, G. Hoffmann, V. Masson-Delmotte, and F. Parrenin, 2003: Magnitude of isotope/temperature scaling for interpretation of central Antarctic ice cores. *J. Geophys. Res.,* **108,** 4361, doi:10.1029/2002JD002677.

Kavanaugh, J. L., and K. M. Cuffey, 2003: Space and time variation of δ^{18}O and δD in Antarctic precipitation revised. *Global Biogeochem. Cycles,* **17,** 1017, doi:10.1029/2002GB001910.

Kreutz, K. J., and Coauthors, 1999: Seasonal variations of glaciochemical, isotopic and stratigraphic properties in Siple Dome (Antarctica) surface snow. *Ann. Glaciol.,* **29,** 38–44.

Lorius, F., and L. Merlivat, 1977: Distribution of mean surface stable isotope values in East Antarctica: Observed changes with depth in the coastal area. Isotopes and Impurities in Snow and Ice, International Association of Hydrological Sciences, Publication 118, 127–137.

Masson-Delmotte, V., B. Stenni, and J. Jouzel, 2004: Common millennial-scale variability of Antarctic and Southern Ocean temperatures during the past 5000 years reconstructed from the EPICA Dome C ice core. *Holocene,* **14,** 145–151.

McMorrow, A. J., M. A. J. Curran, T. D. Van Ommen, V. I. Morgan, M. A. J. Pook, and I. Allison, 2001: Intercomparison of firn core and meteorological data. *Antarct. Sci.,* **13,** 329–337.

Merlivat, L., and J. Jouzel, 1979: Global climatic interpretation of the deuterium-oxygen 18 relationship for precipitation. *J. Geophys. Res.,* **84** (C8), 5029–5033.

Motoyama, H., N. Hirasawa, K. Satow, and O. Watanabe, 2005: Seasonal variations in oxygen isotope ratios of daily collected precipitation and wind drift samples and in the final snow cover at Dome Fuji Station, Antarctica. *J. Geophys. Res.,* **110,** D11106, doi:10.1029/2004JD004953.

Noone, D., and I. Simmonds, 2002: Associations between $\delta^{18}O$ of water and climate parameters in a simulation of atmospheric circulation for 1979–95. *J. Climate,* **15,** 3150–3169.

North Greenland Ice Core Project Members, 2004: High-resolution record of Northern Hemisphere climate extending into the last interglacial period. *Nature,* **431,** 147–151.

Petit, J. R., J. W. C. White, N. W. Young, J. Jouzel, and Y. Korotkevich, 1991: Deuterium excess in recent Antarctic snow. *J. Geophys. Res.,* **96** (D3), 5113–5122.

Reijmer, C. H., and M. R. Van den Broeke, 2003: Temporal and spatial variability of the surface mass balance in Dronning Maud Land, Antarctica, as derived from automatic weather stations. *J. Glaciol.,* **49,** 512–520.

——, ——, and M. P. Scheele, 2002: Air parcel trajectories and snowfall related to five deep drilling locations in Antarctica based on the ERA-15 dataset. *J. Climate,* **15,** 1957–1968.

——, E. Van Meijgaard, and M. R. Van den Broeke, 2005: Evaluation of temperature and wind over Antarctica in a Regional Atmospheric Climate Model using one year of automatic weather station data and upper air observations. *J. Geophys. Res.,* **110,** D04103, doi:10.1029/2004JD005234.

Robin, G., 1983: The climatic record from ice cores. *The Climatic Record in Polar Ice Sheets,* G. Robin, Ed., Cambridge University Press, 180–195.

Roeckner, E., and Coauthors, 1996: The atmospheric general circulation model ECHAM-4: Model description and simulation of present-day climate. MPI Tech. Rep. 218, Max Planck Institute for Meteorology, 90 pp.

Scheele, M. P., P. C. Siegmund, and P. F. J. Van Velthoven, 1996: Sensitivity of trajectories to data resolution and its dependence on the starting point: In or outside a tropopause fold. *Meteor. Appl.,* **3,** 267–273.

Schmidt, G. A., G. Hoffmann, D. T. Shindell, and Y. Hu, 2005: Modeling atmospheric stable water isotopes and the potential for constraining cloud processes and stratosphere-troposphere water exchange. *J. Geophys. Res.,* **110,** D21314, doi:10.1029/2005JD005790.

Schneider, D. P., E. J. Steig, and T. Van Ommen, 2005: Interpretation of high resolution ice core stable isotopic records from Antarctica: Towards interannual climate reconstruction. *Ann. Glaciol.,* **41,** 63–70.

Stenni, B., V. Masson-Delmotte, S. Johnsen, J. Jouzel, A. Longinelli, E. Monnin, R. Röthlisberger, and E. Selmo, 2001: An oceanic cold reversal during the last deglaciation. *Science,* **293,** 2074–2077.

Stohl, A., G. Wotawa, P. Seibert, and H. Kromp-Kolb, 1995: Interpolation errors in wind fields as a function of spatial and temporal resolution and their impact of different types of kinematic trajectories. *J. Appl. Meteor.,* **34,** 2149–2165.

Tiedtke, M., 1993: Representation of clouds in large-scale models. *Mon. Wea. Rev.,* **121,** 3040–3061.

Van de Berg, W. J., M. R. Van den Broeke, C. H. Reijmer, and E. van Meijgaard, 2006: Reassessment of the Antarctic surface mass balance using calibrated output of a regional atmospheric climate model. *J. Geophys. Res.,* **111,** D11104, doi:10.1029/2005JD006495.

Van den Broeke, M. R., 1997: Spatial and temporal variation of sublimation on Antarctica: Results of a high-resolution general circulation model. *J. Geophys. Res.,* **102** (D25), 29 765–29 777.

——, J.-G. Winther, E. Isaksson, J. F. Pinglot, L. Karlöf, T. Eiken, and L. Conrads, 1999: Climate variables along a traverse line in Dronning Maud Land, East Antarctica. *J. Glaciol.,* **45,** 295–302.

Van Lipzig, N. P. M., E. Van Meijgaard, and J. Oerlemans, 2002a: The effect of temporal variations in the surface mass balance and temperature-inversion strength on the interpretation of ice-core signals. *J. Glaciol.,* **48,** 611–621.

——, ——, and ——, 2002b: The spatial and temporal variability of the surface mass balance of Antarctica: Results from a regional atmospheric climate model. *Int. J. Climatol.,* **22,** 1197–1217.

——, J. C. King, T. A. Lachlan-Cope, and M. R. Van den Broeke, 2004: Precipitation, sublimation, and snow drift in the Antarctic Peninsula region from a regional atmospheric model. *J. Geophys. Res.,* **109,** D24106, doi:10.1029/2004JD004701.

Van Ommen, T. D., and V. Morgan, 1997: Calibrating the ice core paleothermometer using seasonality. *J. Geophys. Res.,* **102** (D8), 9351–9357.

Waddington, E. D., E. J. Steig, and T. A. Neumann, 2002: Using characteristic times to assess whether stable isotopes in polar snow can be reversibly deposited. *Ann. Glaciol.,* **35,** 118–124.

Werner, M., and M. Heimann, 2002: Modeling interannual variability of water isotopes in Greenland and Antarctica. *J. Geophys. Res.,* **107,** 4001, doi:10.1029/2001JD900253.

——, U. Mikolajewicz, M. Heimann, and G. Hoffmann, 2000: Borehole versus isotope temperatures on Greenland: Seasonality does matter. *Geophys. Res. Lett.,* **27,** 723–726.

——, M. Heimann, and G. Hoffmann, 2001: Isotopic composition and origin of polar precipitation in present and glacial climate simulations. *Tellus,* **53B,** 53–71.

Zwally, H. J., M. Giovinetto, M. Craven, V. Morgan, and I. Goodwin, 1998: Areal distribution of the oxygen-isotope ratio in Antarctica: Comparison of results based on field and remotely sensed data. *Ann. Glaciol.,* **27,** 583–590.